FLOMEKO2019
18th International Flow Measurement Conference
Portugal | Lisbon | LNEC | 26-28 june 2019

Non-Nulling Measurements of Flue Gas Flows in a Coal-Fired Power Plant Stack

A. N. Johnson[1], I. I. Shinder[1], J. B. Filla[1], J. T. Boyd[1], R. Bryant[1], M. R. Moldover[1], T. D. Martz[2]
[1]NIST 100 Bureau Drive, Gaithersburg, MD, USA
[2]EPRI, 3420 Hillview Ave., Palo Alto, CA 94304
(corresponding author): Aaron.Johhson@nist.gov

Exhaust flows from coal-fired stacks are determined by measuring the flue gas velocity at prescribed points in the stack cross section. During the last 30+ years these velocity measurements have been made predominantly using S-type pitot probes. These probes are robust and inexpensive; however, S-probes measure only two components of the velocity vector and can give biased results if the stack flow has significant yaw and pitch angles. Furthermore, S-probe measurements are time intensive, requiring probe rotation (or nulling) at each traverse point to find the yaw angle. The only EPA-sanctioned alternatives to the S-probe are 5-hole probes (i.e., the prism probe and spherical probe) that also require yaw-nulling. We developed a non-nulling technique applicable to the spherical probe and two custom designed 5-hole probes that reduce testing time and may improve measurement accuracy. The non-nulling technique measures all 3 components of velocity without rotating the probe. We assessed the performance of these 5-hole probes in a coal-fired stack at the high-load (16 m/s) and the low-load (7 m/s). For the spherical probes, the non-nulling results and the nulling results were in excellent mutual agreement (< 0.1 %). For the custom probes, the non-nulling and nulling results were inconsistent: the differences were 5% at the high load and 10 % at the low load. We speculate that the nulling data for the custom probes were flawed because the non-nulling data for all the probes accurately determined the yaw and pitch angles at high and low loads. Our results demonstrate that the non-nulling technique can accurately measure flue gas flows in a coal-fired stack.

Introduction

This Introduction briefly reviews (1) the need for accurately measuring flue gas flows, (2) the current "nulling" technique for flue gas measurements and its problems, (3) the possibility of improved measurements using a non-nulling technique, and (4) the encouraging results from preliminary field tests of a non-nulling technique.

(1) The combustion gases from coal-fired power plants (CFPPs) are exhausted into large diameter (> 5 m), vertically oriented smokestacks, which emit pollutants into the atmosphere. To quantify the amount of pollutants released into the atmosphere, the total flow in these stacks must be accurately measured; however, accurate stack flow measurements are difficult. Stacks are fed by a network of elbows, reducers, fans, *etc*. which generate complex, difficult-to-measure flows. The flue gas itself causes additional difficulties because it can be hot (as high as 120°C), acidic, asphyxiating, and in some cases saturated with water vapor. Nevertheless, accurate measurements of the total flue gas flow are essential to monitor emissions of greenhouse gases (GHGs) and other hazardous pollutants.

Pollutant emissions from CFPPs are quantified by continuous emission monitoring systems (CEMS) permanently installed in the stacks. The CEMS equipment measures the concentration of each regulated pollutant as well as the total flow. Federal regulations require annual calibration of the CEMS flow monitors and concentration equipment. These calibrations are performed using an EPA protocol called a relative accuracy test audit (RATA). The flow portion of the calibration is herein referred to as the flow RATA.

(2) How Stack Flows are Currently Measured
The flow RATA maps the axial stack velocity measured along 2 orthogonal chords in the stack

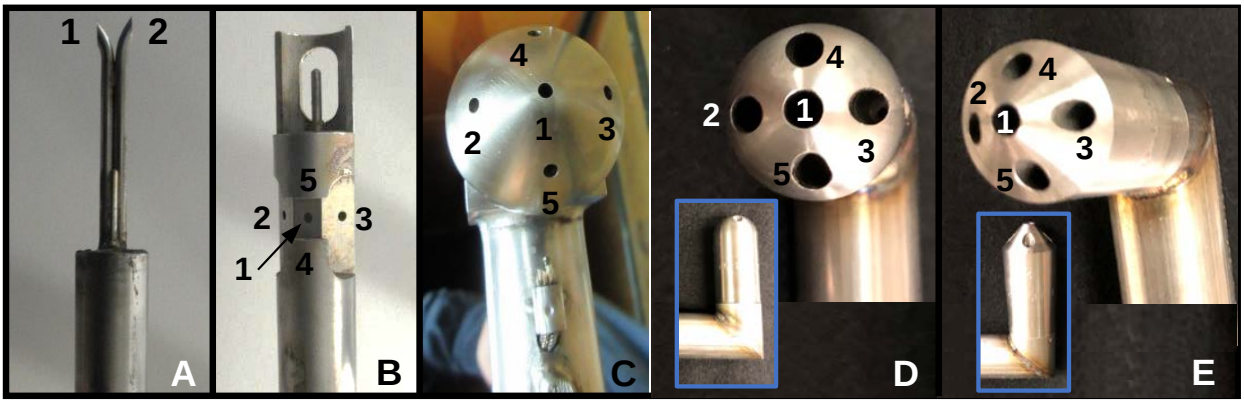

Figure 1. Pictures A, B, and C show the 3 EPA-sanctioned RATA probes including A) the S-probe, B) Prism probe, and C) Spherical Probe. The hemispherical and conical probes shown in D) and E), respectively are custom-made probes designed for non-nulling.

cross-section. A pitot probe is inserted into the flow through ports on the stack wall. On each chord, measurements are made at discrete points located at the centroids of equal area [1]. The discrete velocity measurements are integrated to determine the flow velocity, which in turn, is used to determine the correction factor for the CEMS flow meter.

Figures 1A, 1B, and 1C show the 3 RATA probe types sanctioned by the EPA including A) the S-probe, B) the prism probe, and C) the spherical probe. All 3 probes use the same measurement principle. The axial velocity is correlated to differential pressure measurements made across the probe's pressure ports. Both the prism and the spherical probe have 5 pressure ports and both measure the entire velocity vector including the pitch, yaw, and axial velocity components. In contrast, the S-probe measures only the yaw and axial velocities, and has been shown to give flow velocities that are biased high if significant pitch and yaw are present in the flow [2].

Nulling Method

The 3 EPA-sanctioned probes use a yaw-nulling method [3, 4, 5] to determine the angle of off-axis flow in the yaw direction, which we call the yaw-null angle (β_{null}). At each point on the RATA map, the probe is *nulled* by rotating it about its axis until the vector sum of the yaw and axial velocities align with pressure port 1. For a 3-D probe the nulling procedure can be accomplished in a single rotation. The S-probe requires 2 rotations. First the S-probe is nulled by rotating it about its axis until $P_{12} = 0$. A second 90° rotation orients port 1 so that it faces into the flow. Once the probe is nullled, the probe calibration parameters are used to determine the dynamic pressure (P_{dyn}), and for 3-D probes the pitch angle (α).

Errors Due to Imperfect Nulling

If the null condition is not satisfied, significant flow measurement errors can occur. The nulling errors increase with the ratio $\Delta P_{null}/P_{dyn}$, where the null-differential-pressure $\Delta P_{null} = P_{23}$ for 3-D probes and $\Delta P_{null} = P_{12}$ for the S-probe. The errors become significant when $\Delta P_{null}/P_{dyn}$ is not small relative to unity [6]. In most cases the nulling procedure is performed manually. A person rotates the probe while reading a differential pressure gauge to determine the exact yaw angle for which $\Delta P_{null} = 0$. However, transients in stack flows, noisy pressure signals, and human errors make nulling imperfect and introduce unquantified bias (*e.g.* high for an S-probe) into the measurement process.

When the velocity field has a significant yaw component, nulling the probe can be

time-intensive and, consequently, expensive. When mapping the flow field, several iterations are generally required to find the yaw-null angle at each traverse point. The nulling time increases in wet stacks since stack testers must frequently interrupt the measurement process to purge the probe's pressure ports of droplets or particles. Because 3-D probes have more pressure ports than S-probes, and because the diameters of these ports are smaller than the ports of S-probes, 3-D probes are more susceptible to plugging. Consequently, 3-D probes generally require more time than the S-probe to complete the flow RATA. Historically the stack flow measurement community has opted to use the more robust and economical, but less accurate, S-probe.

(3) Non-Nulling Method

Non-nulling methods determine the axial velocity without rotating the probe at each traverse point to find β_{null}. Instead, the axial velocity, the pitch angle, and the yaw-null angle β_{null} are determined with the probe oriented at zero yaw angle (*i.e.*, $\beta = 0°$ such that port 1 on the probe is aligned with the stack axis). Compared with nulling methods, non-nulling methods reduce the time needed to perform flow RATAs. CFFPs are concerned about the duration of flow RATAs because they must maintain loads stipulated by the RATA instead of loads dictated by customer supply and demand.

The non-nulling method also has the potential to improve flow measurement accuracy compared with nulling methods. First, the S-probe measures only 2 components of the velocity vector while the non-nulling method applies to 3-D probes and thereby measures the entire velocity vector. Second, Method 2F [5], which is the EPA nulling method for 3-D probes, does not address errors resulting from imperfect nulling, as discussed above.

In this manuscript we demonstrate the feasibility of accurately determining the total flow in a CFPP stack using a non-nulling method and commercially available flow RATA equipment. In previous work, we achieved 1 % accuracy when we performed flow RATAs in NIST's Scale-Model Smokestack Simulator (SMSS) using a spherical probe, even with highly-distorted flows [7, 8]. However, the SMSS facility uses ambient air as surrogate for flue gas and performs flow RATAs under laboratory conditions using laboratory grade instrumentation.

Using NIST's wind tunnel and NIST's smokestack simulator, we developed non-nulling algorithms for the spherical probe in Fig. 1C and for the 2 custom probes shown in Figs. 1D and 1E. At NIST, we calibrated these probes using our non-nulling method and also EPA's Method 2F, and then we used these probes to measure the flow velocity in a CFPP stack.

For assessing the accuracy and limitations of the non-nulling method, we selected a CFPP stack known to have complex flows. The selected stack's RATA measurement platform was only 3.8 stack diameters ($D = 6.8$ m) downstream of a 90° elbow. Moreover, upstream of the elbow, flow from two wet scrubbers merged into a single stream. Not surprisingly, the flow at the RATA platform had significant yaw-null angles that were nearly -30° at the stack wall. The flue gas was saturated with water from the wet scrubbers. The wet, particle-laden gas frequently plugged the 3-D probes; plugging increased the duration of the tests and resulted in false high (or low) axial velocity measurements both for Method 2F and the non-nulling method. We developed a statistical method based on the noisiness of the measured pressure signals to identify data affected by plugging.

The CFPP stack was equipped with an X-pattern ultrasonic flow meter system, which was used as the CEMS flow monitor. The CFPP provided us with minute by minute CEMS flow velocity data (V_{CEMS}) for the duration of the test. On average, the stability of V_{CEMS} during the flow RATAs was better than 1.5 %. We performed a 16-point flow RATA

using both Method 2F and the non-nulling method. The flow RATAs were performed at two loads, a high load with a flue gas velocity of 16 m/s, and at a low load of 7 m/s.

Table 1. Normalized flow velocity (V_{RATA}/V_{CEMS}) for Method 2F (M2F) and for the non-nulling method at zero yaw angle (NN, $\beta = 0$) at a high load of 16 m/s and a low load of 7 m/s.

Probe Types	Load (Repeats)	M2F	NN ($\beta = 0$)	M2F/NN -1
Spherical Probes (SP)	High (4)[a]	0.993 (2.1 %)[b]	0.994 (0.4 %)[b]	-0.1 %[c]
Custom Probes (CP)	High (4)	1.053 (0.4 %)	0.990 (0.7 %)	+5.9 %
CP/SP-1	High	6.0 %	-0.4 %	
Spherical Probes (SP)	Low (6)	1.02 (1.3 %)	1.02 (1.7 %)	0 %
Custom Probes (CP)	Low (6)	1.108 (2.0 %)	0.997 (1.6 %)	+10 %
CP/SP-1	Low	8.6 %	-2.3 %	

a) Number of repeated RATA traverses for the same probe at the same flow

b) Standard deviation of normalized RATA velocity expressed as a percent

c) Percent difference computed using 100 (M2F/NN -1)

(4) The CFPP test results are summarized in Table 1. The tabulated RATA velocities are normalized by the CEMS velocity (V_{RATA}/V_{CEMS}) to help account for flow variations during and between measurements. The data in column "M2F" are the normalized flow velocities for Method 2F; the data in column "NN ($\beta = 0$)" are the normalized non-nulling velocities obtained with the probe at a zero yaw angle.

There are 4 primary results. First, the non-nulling method and Method 2F showed excellent agreement for the spherical probes. As indicated in the last column, the difference at high load was -0.1 % and at low load the difference was 0 %.

Second, the flow results from the non-nulling method were consistent throughout the test. The percent difference of V_{NN}/V_{CEMS} determined with the spherical probes and the custom probes was only -0.4 % at high load and -2.3 % at low load.

Third, V_{NN}/V_{CEMS} is close to unity in all cases. This agreement between V_{NN} and V_{CEMS} is better than expected. The values of V_{CEMS} are based on an earlier S-probe RATA calibration that used the conventional nulling method. Our values of V_{NN} are based on a 16-point traverse that did not account for the lower velocities near the wall. If we had accounted the lower velocities, we would have found $V_{NN} < V_{CEMS}$. Note: we measured pitch angles less than 5°, so that S-probe errors related to pitch angle are negligible in this stack.

Fourth, the results of Method 2F and the non-nulling method showed poor agreement for the custom probes: the differences are 5.9 % at high load and 10 % at low load. Presently we do not understand the cause of the differences. However, we suspect these results are erroneous for the following reasons: a) the non-nulling results were consistent for all tests and agreed with the results obtained with the EPA-sanctioned spherical probe, b) in cases where RATAs based on Method 2F disagree with the S-probe nulling method, the Method 2F results are typically lower due to inherent positive biases in the S-probe [9].

Probe Calibrations in NIST's Wind Tunnel

We calibrated all 3 probe types in NIST's wind tunnel using both Method 2F [5] and the non-nulling method. Calibrations were performed in the wind tunnel's rectangular test section (1.5 m × 1.2 m) using NIST's Laser Doppler Anemometer (LDA) working standard. The metrological traceability of the LDA working standard is documented in the following references 10, 11, and 12. We use the LDA velocity (U_{LDA}) in conjunction with air density (ρ_{AIR}) in the wind tunnel to determine the dynamic pressure, $P_{dyn} = \rho_{AIR} U_{LDA}^2/2$. The wind tunnel is equipped with an automated traversing system, which positions the pitot probes to prescribed pitch angles (α) and yaw angles (β) in the test section [13, 14]. The expanded uncertainty of wind speed is less than 1 %, and the expanded uncertainties of pitch and yaw angles are 0.5°.

Method 2F Probe Calibrations

We calibrated 4 spherical probes, 2 hemispherical probes, and 2 conical probes. All the probes were calibrated at 11 velocities ranging from 5 m/s to 30 m/s in steps of 2.5 m/s, and at 17 pitch angles ranging from -20° to 20° in steps of 2.5°. Thus, for each probe we measured 187 combined velocity and pitch angle set points. We used *the Curve Fit Method* [6] to determine the pitch calibration factor, F_1, and the velocity calibration, F_2, at the null condition ($P_{23} = 0$). The Curve Fit Method does not require rotating the probe to the exact position where $P_{23} = 0$; instead *the pitch pressure ratio,* P_{45}/P_{12}, and *the velocity pressure ratio*, $[P_{dyn}/P_{12}]^{1/2}$, are measured over a narrow range of yaw pressures surrounding $P_{23} = 0$. By definition, the pitch pressure ratio and the velocity pressure ratio equal the respective calibration factors, $F_1 = P_{45}/P_{12}$ and $F_2 = [P_{dyn}/P_{12}]^{1/2}$ at zero yaw pressure, $P_{23} = 0$.

The measured values of the pitch pressure ratio and the velocity pressure ratio values are fit by either a 2nd or 3rd degree polynomial function of the yaw pressure, which we evaluate at $P_{23} = 0$ to determine the respective null parameters, F_1 and F_2.

Figures 2 and 3 plot the calibration parameters F_1 and F_2 as functions of the pitch angle for a hemispherical probe (Fig. 1D) and a conical probe (Fig. 1E). The circles (○) are data taken at the 11 different velocities ranging from 5 m/s to 30 m/s. For both probes, F_1 is nearly independent of velocity, but F_2 exhibits a small, systematic velocity dependence. The solid lines (—) are curves fitted to the data. The pitch angle (α) is fitted by a 6th degree polynomial of independent variable F_1, and F_2 is fit to 6th degree polynomial of α.

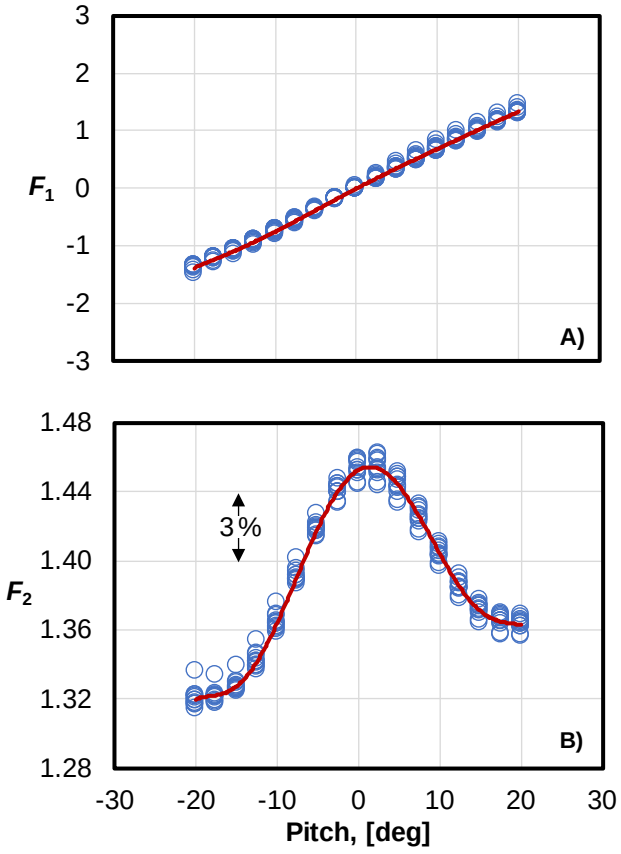

Figure 2. Hemispherical probe F_1 and F_2 calibration parameters plotted versus pitch angle. The circles (○) are data points taken at 11 different velocities and the solid line (—) is a curve fitted to the points.

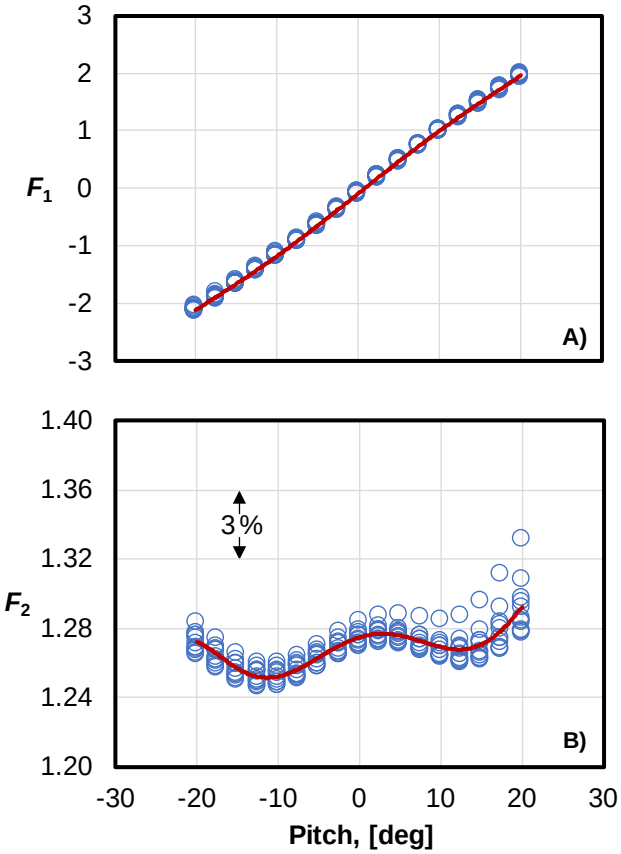

Figure 3. Conical probe F_1 and F_2 calibration parameters plotted versus pitch angle. The circles (○) are data points taken at the 11 different velocities and the solid line (—) is a curve fitted to the points.

As observed in Figs. 2B and 3B, the curve fit of F_2 is essentially an average of the velocity data at each pitch angle. This approximate method of accounting for the velocity dependence is consistent with the Method 2F protocol.

For flow RATAs performed using Method 2F, we determined the axial velocity at each traverse point using the following procedure. First, we nulled the probe and measured the yaw-null angle (β_{null}) with an inclinometer. Next, we determined the pitch calibration factor, $F_1 = P_{45}/P_{12}$, from the measured null pressures P_{45} and P_{12}. We use the 6th degree polynomial determined during calibration, $\alpha = \alpha(F_1)$ (here expressed in generic functional form) to determine α. Then, the calculated α is used to determine the velocity calibration factor using the fitted curve $F_2 = F_2(\alpha)$ developed during calibration. The differential pressure between ports 1 and 2 on the probe head along with the velocity calibration factor determine the dynamic pressure, $P_{dyn} = F_2^2 P_{12}$. Finally, the axial velocity at each traverse point is determined as a function of the 1) dynamic pressure, 2) yaw-null angle, and 3) pitch angle using

$$V_{axial} = \sqrt{\frac{2P_{dyn}}{\rho}} \cos\left(\beta_{null} - \beta_0\right) \cos\left(\alpha\right) \quad (1)$$

where β_0 accounts for any yaw angle offset (or misalignment) when probes are installed into the automated traverse system used to perform the flow RATA. We followed EPA Method 4 to measure the flue gas moisture [15], and we used EPA Method 3A to determine the molar mass [16]. The flue gas density (ρ) was determined *via* Method 2F using pressure, temperature, and molar mass measurements.

Non-Nulling Probe Calibrations

The non-nulling method also uses Eq. (1) to determine the axial velocity at each traverse point. The fundamental difference is that P_{dyn}, β_{null}, and α are determined by fitting 3000 or more data points acquired in NIST's wind tunnel. These data span velocities from 5 m/s to 30 m/s, pitch angles from -20° to 20°, and yaw angles from -42° to 42°. The fitted calibration curve is a fifth-degree polynomial of the four independent variables: P_{12}, P_{13}, P_{14}, and P_{15}.

For the non-nulling method, there is no need to rotate the probe. However, since scenarios could arise where rotating the probe is beneficial (*e.g.*, the predicted value of β_{null} exceeds the curve fit limits), we discuss a more general application of the non-nulling method. First the probe is rotated to a user-selected yaw angle (β). Next, we simultaneously measure the four input pressures: P_{12}, P_{13}, P_{14}, and P_{15}, and use the non-nulling calibration curve fits to calculate P_{dyn}, β'_{null}, and α. Here, β'_{null} is the calculated yaw-null angle relative to the rotated probe position at β. The absolute yaw-null angle is the sum of the probe yaw angle and the yaw-null angle determined from the non-nulling algorithm,

$$\beta_{null} = \beta + \beta'_{null} . \quad (2)$$

If the probe is oriented at a zero yaw angle ($\beta = 0°$), then the yaw-null angle determined by the non-nulling algorithm equals the yaw angle measured from the stack axis, $\beta'_{null} = \beta_{null}$. Alternatively, if one rotates the probe to the yaw-null angle, $\beta = \beta_{null}$, then β'_{null} would be zero, ideally. In this case any changes in β'_{null} would provide an indication of how the yaw-null angle fluctuates while the probe is oriented at the yaw-angle.

Test Protocol for Stack Flow Measurements

We conducted 16-point flow RATAs using multiple probe types. We used a set of 4 spherical probes (see Fig. 1C), and we also used a combination of the 2 custom probes shown in Fig. 1D and 1E. We tested each probe type at 2 loads, a high load with a nominal flow velocity of 16 m/s, and a low load of 7 m/s. The test matrix shown in Table 2 lists the probes used for each test, the flow loads, and the number of repeated runs. The diagram in Fig. 4 shows the cross-sectional view of the setup. The probe installed in each port measures the axial velocity of the nearest 4 points as illustrated in the figure. A complete traverse, herein called a *run*, includes all 16 points shown in the figure. We completed 4 runs for each probe type at the high load and 6 runs for each probe type at the low load.

Table 2. Test matrix for 16-point flow RATAs performed in CFPP stack.

Test No.	Probe Types	Load	Repeat Runs	Port 1	Port 2	Port 3	Port 4
1	Spherical Probes	High	4	Sphere 2	Sphere 3	Sphere 5	Sphere 6
2	Custom Probes	High	4	Hemi-sphere 1	Conical 1	Hemi-sphere 1	Conical 2
3	Custom Probes	Low	6	Hemi-sphere 1	Conical 1	Hemi-sphere 1	Conical 2
4	Spherical Probes	Low	6	Sphere 2	Sphere 3	Sphere 5	Sphere 6

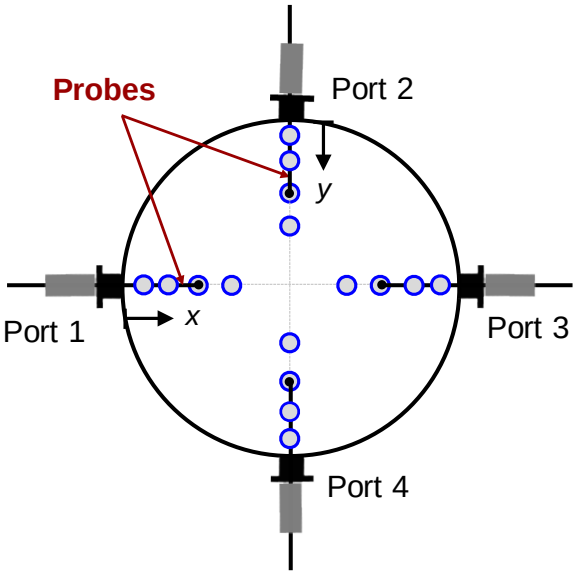

Figure 4. Cross-section of stack showing probes, port numbers and 16 traverse points located at centroids of equal stack area.

Our test protocol was conducted by an EPRI contractor who used commercially available RATA equipment called "Multiple Automated Probe System" (MAP)[1] to perform five functions: 1) move all 4 probes simultaneously to specified points; 2) periodically supply high pressure gas to purge droplets or particles plugging any of the 5 pressure ports on the probe head; 3) send a dc voltage to our data acquisition system 5 s prior to starting a purge, 4) implement the Method 2F nulling procedure including the measurement of β_{null} and β_0; and 5) provide time stamps at the start and stop of each non-nulling and Method 2F measurement intervals.

Data Acquisition System

To collect non-nulling and Method 2F data, we designed and assembled four custom data acquisition systems that were connected to a single laptop computer. Each system included inexpensive, industrial-grade differential pressure transducers, which we sampled at 10 Hz. The transducers were bidirectional with a full-scale of 1244 Pa and a time response faster than 1 kHz. We used pneumatically actuated valves to isolate the differential pressure transducers during purge events. The transducers and valves for each system were housed in a weather-proof case. Each case was placed on the floor of the RATA measurement platform just below the port where the corresponding probe was installed. Each case contained 5 pressure transducers that were connected to the 5 pressure ports on the 3-D probe using 6.35 mm inner diameter tubes approximately 13 m long. In this way, we measured the flue gas pressure (minus a near ambient reference pressure, P_{ref}, located inside the case) at all 5 pressure ports on the probe

1 Certain commercial equipment, instruments, or materials are identified in this report to foster understanding. Such identification does not imply recommendation or endorsement by the National Institute of Standards and Technology, nor does it imply that the materials or equipment identified are necessarily the best available for the purpose.

head. The required differential pressures for the non-nulling algorithm (*i.e.,* P_{12}, P_{13}, P_{14}, P_{15}) and for Method 2F (*i.e.,* P_{23}, P_{12}, P_{45}) were calculated by subtracting the appropriate pressure measurements. For example, the yaw pressure was determined by subtracting the measured pressures on port 2 from port 3, $P_{23} = (P_2 - P_{ref}) - (P_3 - P_{ref})$.

Procedure for Automated Traverses

Each of the 4 tests listed in Table 2 began by starting the data acquisition unit. Pressure data were collected throughout the test except during purge events, which occurred approximately once every minute. During purge events, valves isolated the transducers from the purge pressure while simultaneously re-zeroing the transducers to the common reference pressure.

The same measurement protocol was followed at each traverse point. The MAP system simultaneously moved the 4 probes to the specified traverse point and rotated each probe to a zero yaw angle. After a 3 s stabilization period, the axial velocity ($V_{NN@0yaw}$) was measured for 10 s using the non-nulling algorithm. Next, the MAP system nulled each probe and recorded its β_{null}. After another 3 s stabilization period we measured the axial velocity for 10 s via Method 2F (V_{M2F}) and the non-nulling method ($V_{NN@null}$). Thus, we measured 3 velocities at each traverse point: 1) non-nulling with the probe at zero yaw; $V_{NN@0yaw}$, 2) Method 2F at the yaw-null angle; V_{M2F}, and 3) a second non-nulling measurement coincident with V_{M2F} where the probe is oriented at the yaw-null angle; $V_{NN@null}$. The second non-nulling measurement provided insight regarding the steadiness of the yaw-null angle, and could be directly compared to V_{M2F} since both measurements were made simultaneously.

Data Processing

The 3 axial velocities (*i.e.*, $V_{NN@0yaw}$, V_{M2F}, and $V_{NN@null}$) measured at each traverse point are all calculated using Eq. (1). However, the algorithms for determining P_{dyn}, β_{null}, and α differ for the non-nulling method and Method 2F. The calculations for both methods are outlined above in the section entitled *Probe Calibrations*. In this section, we emphasize the different approach in averaging the data in each 10 s collection interval.

Method 2F determines the average axial velocity and pitch angle from *pressure averages.* Specifically, we calculated $P_{12,avg}$ and $P_{45,avg}$, which are arithmetic averages of P_{12} and P_{45} sampled at 10 Hz for 10 s.

In contrast, our implementation of the non-nulling method determines the average dynamic pressure (P_{dyn}), yaw-null angle (β_{null}), and pitch angle (α) from *time averages*. These quantities are calculated every 0.1 s when P_{12}, P_{13}, P_{14}, and P_{15} are updated. At the end of the 10 s collection interval, we calculate the arithmetic average of the 100 values of P_{dyn}, β_{null}, and α. As expected for the steady flows in NIST's wind tunnel, the values of P_{dyn}, β_{null}, and α computed from the pressure averages and the time averages were indistinguishable. If transients are present in the stack flow, a time average may be more accurate than a pressure average. In the CFPP stack, we compared the axial velocities V_{axial} determined from pressure averages and time averages in a few cases. For most of the comparisons, the values of V_{axial} agreed to better than 1 %; in a few cases V_{axial} differed by 10 % or more.

One disadvantage of time-averaging is that the noisy pressure signals occasionally yielded values of P_{dyn}, β_{null}, or α that exceed the limits of the non-nulling calibration curve. This problem was unexpected; we circumvented it by excluding the anomalous values from the averages. Fortunately, there were only a few cases where the calculated average did not include at least 80 % of the data. In future tests we will expand the range of the non-nulling calibration curve and we will retake data points that do not include at

least 80 % (or some user-specified percentage) of data in the time averages.

Unfortunately, the data acquisition was not set up to process data during the CFPP stack measurements. Therefore, we processed the data after the field tests were completed. We used the time stamps provided by the MAP system to identify the non-nulling and Method 2F pressure data. For the low loads, approximately 20 % of the data could not be found at the indicated time stamps. At the high load less than 5 % of the data was unaccounted for.

Results

Table 1 summarizes the average flow results. It provides solid evidence that the non-nulling method has the potential to make efficient, accurate stack flow measurements. Because we already discussed the averaged flow data, we now compare the profiles of velocity, yaw-null angle, and pitch angle determined by Method 2F to those determined by the non-nulling method. In addition, we describe how we used the noisy pressure signals to troubleshoot plugging problems.

The flow RATAs were performed along 2 orthogonal axes. We denote the axis extending from port 1 to port 3 in Fig. 4 as the "*x*-axis". The *y*-axis extended from port 2 to port 4. Each axis included 8 traverse points. The traverse points are located at the centroids of equal area, so that flow velocity of each run is calculated by averaging the axial velocities measured at 16 traverse points [1]. The axial velocity, yaw-null angle, and pitch angle are plotted on the *x*/*D* and *y*/*D* axes, respectively, where *D* is the diameter of the stack.

Axial Velocity Profiles

Figures 5A and 5B show that while the load remained constant, the flow profile had large variations (greater than 10 %) at particular locations. Figure 5 is a plot of the normalized axial velocity (V_{RATA}/V_{CEMS}) measured using the spherical probes at high load as functions of *x*/*D* and *y*/*D*, respectively. The open circles (○) connected by dashed lines are Method 2F data from each of the 4 runs. The spacings between the dashed lines indicate profile variations. Despite these variations, the flow velocity of each Method 2F run is stable as shown in Table 3. The standard deviation expressed as a percent was only 2.1 %.

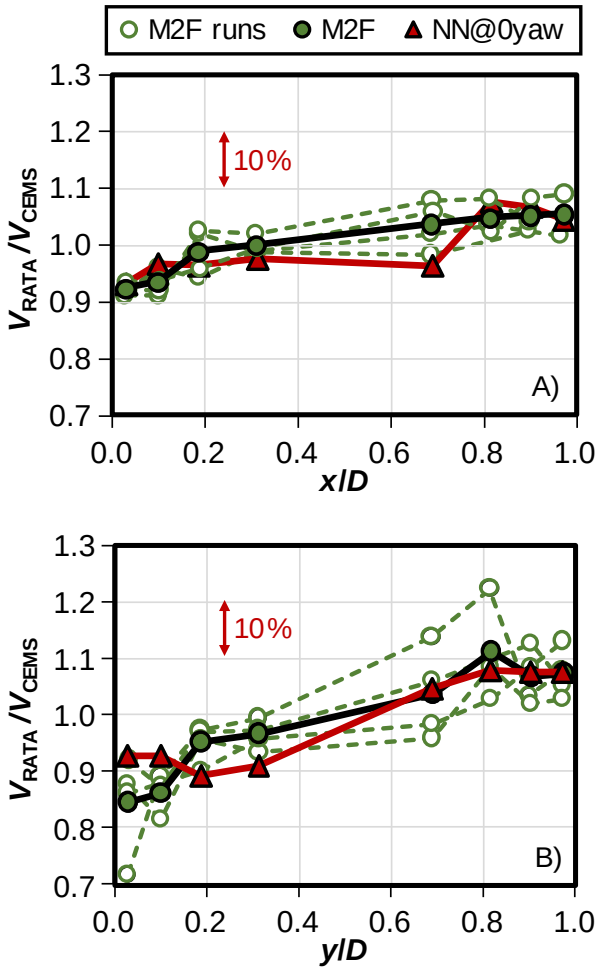

Figure 5. Flow RATA for spherical probes at high load: Plots of normalized axial velocity versus A) *x*/*D,* and B) *y*/D.

We observed similar profile variations (not plotted) in the 4 non-nulling runs even though the standard deviation of the average velocity was only 0.4 %.

The localized variations in the flow field indicated in Figs. 5A and 5B might be due to vortices. We are confident that they are not artefacts of the measurements (*e.g.*, caused by plugging or filtering the data) because the average flow velocity for each run is stable.

The solid circles (●) and solid triangles (▲) in Fig. 5 are the averages of the Method 2F runs and the non-nulling runs, respectively. In Figs. 5A and 5B the solid lines connecting the averaged points are close to each other. This displays the good agreement of the Method 2F velocity profiles with the non-nulling velocity profiles. Table 3 shows that the difference in the averaged flow velocity is only -0.1 %. We emphasize that the normalized velocity profiles measured at both high and low loads were similar to the profiles observed in Figs. 5A and 5B.

Table 3. Normalized flow velocities determined by Method 2F and by the non-nulling method for the 4 repeated runs measured with spherical probe at high load (16 m/s).

Run No.	$\frac{V_{M2F}}{V_{CEMS}}$	$\frac{V_{NN@0yaw}}{V_{CEMS}}$	% Diff[c]
1	1.008	0.999	0.9 %
2	1.009	0.993	1.6 %
3	0.965	0.991	-2.6 %
4	0.988	0.992	-0.4 %
Avg[a]	**0.993**	**0.994**	**-0.1 %[c]**
%Std Dev[b]	**2.1 %**	**0.4 %**	

a) Avg is the average of the 4 runs

b) %Std Dev is 100 times the standard deviation of the 4 runs dividing by the average

c) %Diff is calculated by $100(V_{M2F}/V_{NN@0yaw}-1)$

Yaw Angle Profiles

Figure 6 shows the average yaw-null profiles for the spherical probe at high load. The Method 2F (●) and non-nulling (▲) yaw-null angles show the same trend and are in good agreement in Figs. 6A and 6B. Both methods show the magnitudes of yaw-null angles are largest near the wall with a value of nearly 30°. The magnitude yaw-null angle decreases monotonically as one moves away from the wall toward the center of the stack. The differences between Method 2F and the non-nulling method are smallest near the center of the stack and increase to maximum of approximately 7° near the wall in the worst case.

We found that the yaw-null profiles were nearly identical at low load. We obtained the same trends shown in Figs. 6A and 6B independent of probe type (*i.e.*, spherical or custom) and method (*i.e.*, non-nulling or Method 2F).

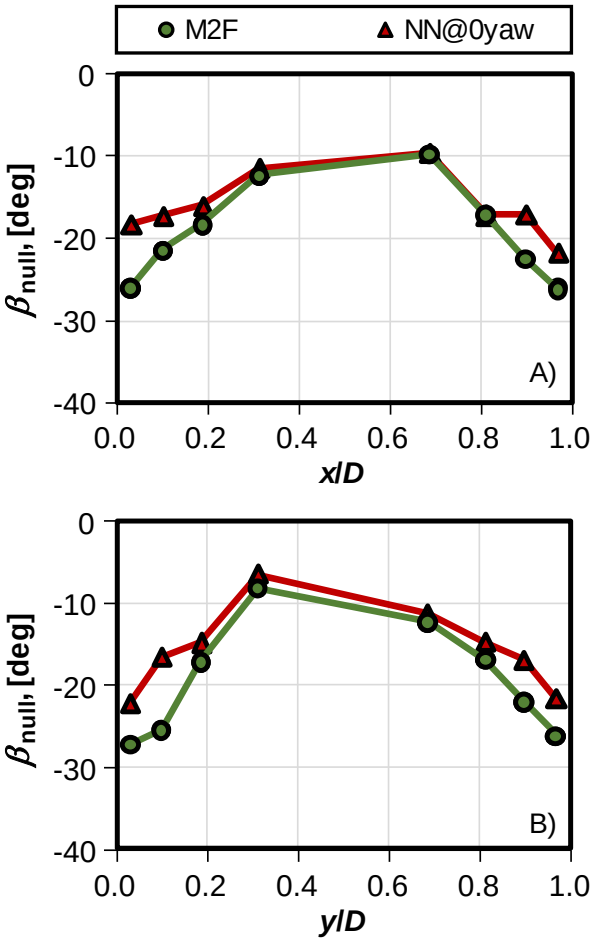

Figure 6. Yaw-null profiles determined using Method 2F (●) and non-nulling with $\beta = 0°$ (▲) along A) port 1 to port 3, and B) port 2 to port 4.

Figure 7 plots the yaw-null angle during a typical 10 s collection time with the probe oriented at $\beta = \beta_{null}$. Because the probe was nulled, the non-nulling algorithm measures β'_{null} defined by Eq. (2). In a steady flow with low turbulence β'_{null} would have a constant value close to 0° during the 10 s collection. In contrast, we observed (Fig. 7) the sine-like oscillations with an amplitude of nearly 30°

and a period of approximately 4 s. Surprisingly, the integrated average of β'_{null} is -1.5°, which is close to zero. This time-dependence of β'_{null} is evidence that the flow field in the CFPP stack had large transients. (Figs. 5A and 5B are additional evidence for large transients.) We note that better averages could be obtained by averaging over more cycles (*i.e.*, longer collection times) or by averaging over the 4 s period. However, since the focus of this work is to demonstrate the feasibility of the non-nulling method, we did not implement this strategy.

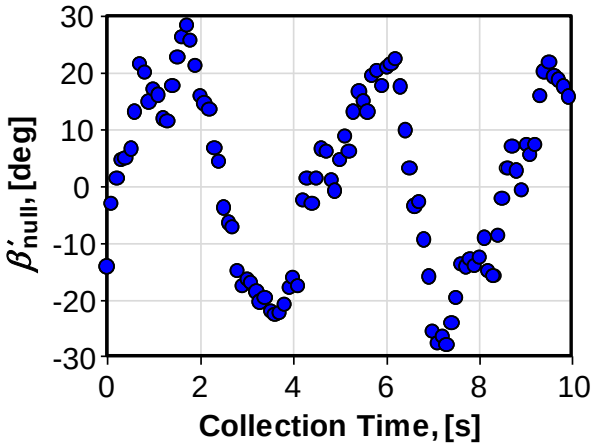

Figure 7. Sine-like oscillations of Yaw-null angle during 10 s Method 2F data collection. (Spherical probe is oriented at the yaw-null angle, and β'_{null} is determined every 0.1 s using the non-nulling algorithm.)

Pitch Angle Profiles

Figures 8A and 8B show profiles of the pitch angle determined by Method 2F (●) and by the non-nulling algorithm with $\beta = 0°$ (▲). These results correspond to Test #1 specified in Table 2. The pitch angles determined by Method 2F and by the non-nulling algorithm agree with each other and have similar, asymmetric dependences on *x*/*D* and *y*/*D*. We found the same characteristic profiles independent of flow load, probe type, and method. Although we hoped to perform the test in a stack with high pitch, the largest pitch angle was only about 5°.

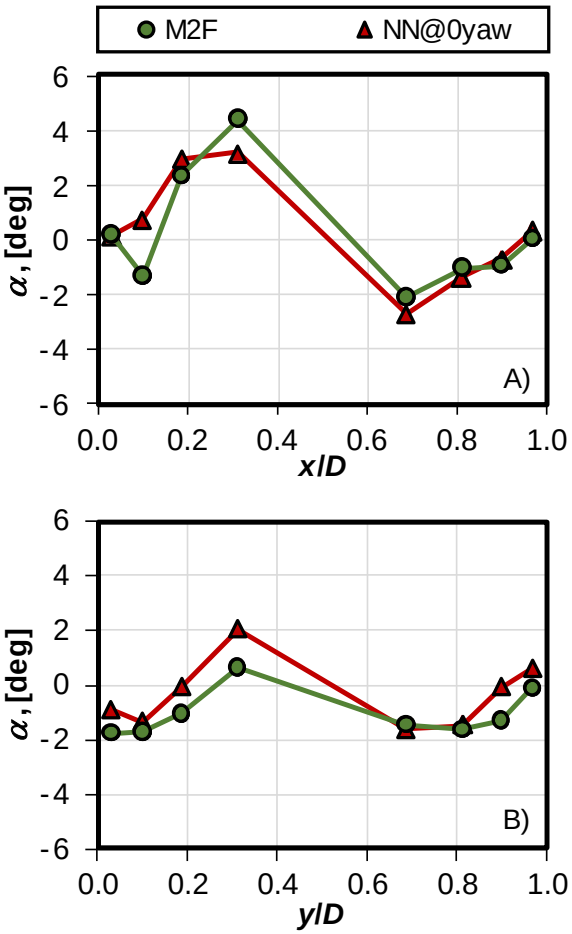

Figure 8. Pitch angle profile for Test #1 in Table 2 where A) *x*/*D* is the dimensionless distance from port 1 to port 3, and B) *y*/*D* is the dimensionless distance from port 2 to port 4.

Troubleshooting Plugging Problems

To mitigate plugging we purged the probe pressure ports every 60 s. Nevertheless, we still had problems with plugging. Plugging issues were most severe for spherical probe 2 during Test #4 in Table 2. The 4 traverse points in port 1 seemed to be the most impacted by plugging problems.

One way to detect plugging is to evaluate the consistency of repeated axial velocity measurements made at the same traverse point. If significant deviations are found at the same traverse points from run to run, then plugging could be the culprit. However, we could not be sure if deviations resulted from plugged pressure ports or from flow transients like those observed in Figs. 5A and 5B. In this

study we used a simple statistical approach to find outliers in the data caused by plugging.

The pressure signals ($P_{n,ref}$; n = 1 to 5) for the five pressure ports on the probe head were noisy. That is, pressures fluctuations during non-nulling and during Method 2F were usually larger than the mean of the pressure signal. We hypothesized that the noise would significantly decrease if a pressure port on the probe head was plugged. For each 10 s collection time, we computed the standard deviation of the pressure signal from each pressure port on the probe head. If the standard deviation was below the typical noise level by a statistically defined threshold, we assumed that the port was plugged.

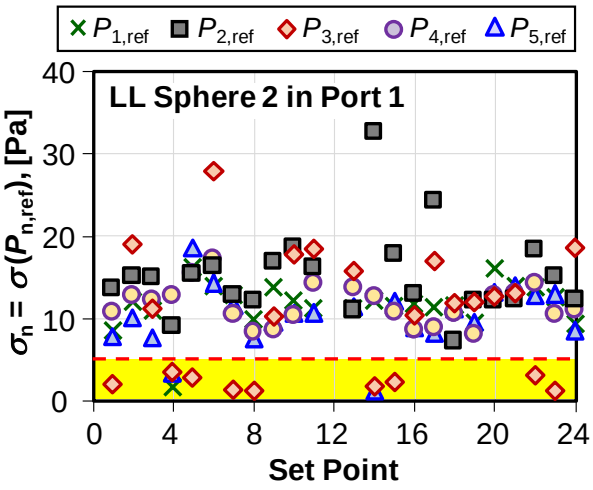

Figure 9. Standard deviation of pressure signals (σ_n) at n = 1 to 5 pressure ports on the spherical probe head. Values of σ_n below the dashed line (– –) indicate that port n was plugged.

Figure 9 illustrates how we applied the statistical approach to detect plugged pressure ports. This example focuses on the non-nulling measurements made at low load using spherical probe 2. The 24 set points on the *x*-axis correspond to the 4 traverse points for port 1 multiplied by the 6 repeated runs (see Test #4, Table 2). The *y*-axis is the standard deviation of the pressure signals $\sigma_n = \sigma(P_{n,ref})$ measured at the n = 1 to 5 pressure ports on the probe head. We considered a pressure port plugged if the standard deviation was below the statistical limit indicated by the dashed line (– –). For simplicity Fig. 9 only shows a single limit; however, in practice we used separate limits for each of the 5 pressure signals. The statistical limit for the nth probe was

$$limit_n = \langle \sigma_n \rangle - k\,\sigma(\sigma_n) \qquad (3)$$

where $\langle \sigma_n \rangle$ is the average of the 24 values of σ_n; $\sigma(\sigma_n)$ is the standard deviation of the 24 values of σ_n; and *k* is the coverage factor which we set equal to 1.5. (The computed normalized velocities had only a weak sensitivity to the value of *k*.)

Figure 10A compares two normalized velocity profiles, one affected by plugging, and the other calculated excluding the subset of data affected by plugging. The figure corresponds to traverses performed at low load using the spherical probes. The velocity (V_{RATA}) was determined using the non-nulling algorithm with the probe oriented at zero yaw angle. Each open triangle (△) is the average of 6 repeated runs. The dashed line connecting the triangles shows the normalized axial velocity profile of the 8 traverse points between port 1 and port 3 (*i.e.*, the x-axis). The first 4 points along *x*/D are traversed by the spherical probe 2 installed in port 1. The statistical approach illustrated in Fig. 9 suggested that several of these points were affected by plugging. If we omit these points when calculating the average axial velocity at each traverse point, we obtain the solid triangles (▲). The solid line connecting the solid triangles shows the normalized velocity profile corrected to account for plugging.

If the normalized velocity profile (▲) in Fig. 10A is correct, we expect to find the same profile at low load independent probe type (*i.e.*, spherical or custom) and independent of the method (*i.e.*, non-nulling or Method 2F). Moreover, for these high Reynolds number flows (3×10^6 to 6.5×10^6) we expect that the high load normalized velocity profile will have essentially the same shape as the low load. Figure 10B

shows that all normalized profiles are in good agreement with the corrected profile. The good agreement of these profiles is 1) strong evidence that we successfully identified and removed data affected by plugging, and 2) that the non-nulling method performed well independent of probe type and flow load.

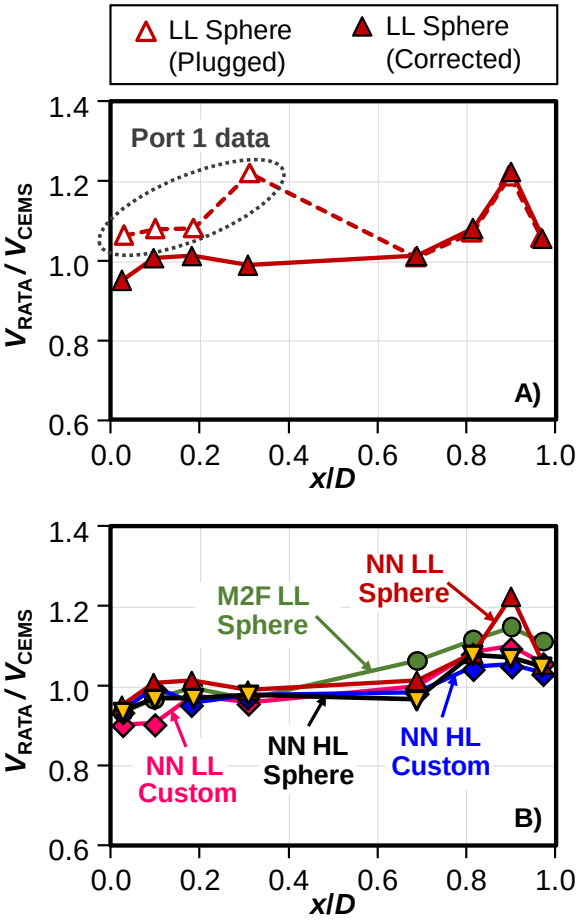

Figure 10. Normalized axial velocity profiles plotted against the dimensionless distance from port 1 to port 3: A) △ Low Load Spherical profile with plugged probe ports; ▲ same profile recalculated with plugged data removed.
B) Five profiles not significantly affected by plugging:
1) ◆ NN LL Custom non-nulling low load,
2) ◆ NN HL Custom non-nulling high;
3) ▼ NN HL Sphere non-nulling high load,
4) ● M2F LL Sphere, Method 2F low load
5) ▲ NN LL Sphere, non-nulling, low load

Conclusions

We demonstrated that the non-nulling method can accurately measure complex flows in CFPP stacks. We conducted 16-point flow RATAs 3.8 stack diameters downstream of the 90° elbow at the stack inlet, and we measured yaw-null angles approaching –30° near the stack wall. We found excellent agreement between the non-nulling method and Method 2F using spherical probes. The results from Table 1 show agreement of -0.1 % at a high load of 16 m/s and 0.0 % at a low load of 7 m/s. We found similar levels of agreement between Method 2F and the non-nulling method when we conducted flow RATAs in NIST Scale-Model Smokestack Simulator (SMSS) [7, 8]. The non-nulling method gives the same flow results but is more time and cost efficient than Method 2F.

The SMSS facility uses air as a surrogate for flue gas and has a 1.2 m diameter test section. The facility can generate complex flows that have yaw-null angles of almost 40° at the wall. The excellent non-nulling flow results found in the SMSS are analogous to those found in this study of a CFPP stack. Thus, the SMSS facility is a satisfactory research facility for characterizing probes used for flow RATAs, ultrasonic CEMS, and other flow monitors for use in CFPP stacks.

We developed custom hemispherical and conical probes and compared their performance in a CFPP stack with the EPA-sanctioned spherical probe using the non-nulling method. The non-nulling flow velocities at high and low loads were consistent for all probe types. After normalizing the measured axial velocities by the CEMS velocity, we found essentially the same characteristic profiles at low and high loads across both orthogonal chords. The normalized Method 2F axial velocities also exhibited the same profiles across the chords.

The non-nulling method measured consistent pitch and yaw-null angles using all the probe types at both high and low loads. Therefore, in future flow RATA testing, a hybrid non-nulling method can be implemented. That is, if while performing a flow RATA using the non-nulling method one has reason to question the axial velocity measurement, the RATA tester can

rotate the probe to the calculated yaw-null angle and take a Method 2F measurement.

The non-nulling method requires bidirectional, fast response differential pressure transducers. We used industrial grade differential transducers for our stack measurements. We measured the pressure (minus a common reference pressure) at each of the 5 ports on the 3-D probe. Pressure measurements were sampled at 10 Hz. They revealed periodic pressure fluctuations with periods ranging between 3 s and 5 s. These transients could not be observed or adequately accounted for (*e.g.*, averaging over the periods) using Method 2F. In contrast, the non-nulling data processing could easily be modified to perform averages over the period.

We used a commercially available automated traverse system 1) to reduce the RATA times and 2) to improve the accuracy of nulling the probes. We emphasize that the benefits of automated traverses are less important for the non-nulling method than for nulling methods because the non-nulling method does not rotate the probe rotation and eliminates errors from imperfect nulling.

Despite purging every 60 seconds, our spherical probes were plagued by plugging that was most severe at low load. We did not experience the same difficulties with the two custom probes; however, we are not sure if this is due to their designs or to good fortune. Additional field tests are needed to better understand plugging.

For accurate flow measurements, it was necessary to distinguish fluctuations of the axial velocity from plugging of one or more pressure ports. We made this distinction by detecting the reduction in the pressure noise that occurs when a pressure port is plugged. Without plugging, the fluctuations of the pressure signals were often larger than their mean values. For each pressure signal, during each 10 s data collection period, we used the standard deviation of the pressure from its mean as a measure of its noise. In this study, we were not prepared to process the noise data in real time. After all the measurements were completed, we used a statistical criterion to discard data corrupted by plugging. In the future, we will process the noise data as they are acquired during a RATA. If the noise indicates plugging the probe can be purged and the data retaken. Thus, the noise measurements will be used as a diagnostic to guide the data acquisition and not to discard data.

In this study we performed a 3000-point calibration on each probe used for the non-nulling measurements. Such an extensive calibration is not practical for routine flow RATAs. Research efforts are underway to determine if a baseline non-nulling calibration can be applied to all probes of the same type. If so, a simple calibration will be done to correct for slight manufacturing differences.

Acknowledgments
We thank John Wright of NIST for his continuing, enthusiastic support of this work. This research was partially funded by NIST's Greenhouse Gas and Climate Science Measurements Program. A Cooperative Research and Development Agreement (CRADA) between NIST and EPRI facilitated our access to a RATA at a CFPP.

[1] Environmental Protection Agency, ***40 CFR Part 60 Application Method 1 Sample and Velocity Traverses for Stationary Sources***, Washington D.C., 1996.

[2] Norfleet, S. K., Muzio L. J., and Martz T. D., ***An Examination of Bias in Method 2 Measurements Under Controlled Non-Axial Flow Conditions***, Report by RMB Consulting and Research, Inc., *May 22, 1998.*

[3] Environmental Protection Agency, ***40 CFR Part 60 Application Method 2 Velocity and S-type Pitot***, Washington D.C., 1996.

[4] Environmental Protection Agency, ***40 CFR Part 60 Application Method 2G Stack***

Gas-Velocity/Volumetric Flow Rate-2D probe, Washington D.C., 1996.

[5] Environmental Protection Agency, 40 CFR Part 60 ***Application Method 2F Stack Gas-Velocity/Volumetric Flow Rate-3D probe***, Washington D.C., 1996.

[6] Shinder, I. I., Johnson, A. N., Moldover, M. R., Filla, B. J., and Khromchenko, V. B., ***Characterization of Five-Hole Probes used for Flow Measurement in Stack Emission Testing,*** 10th International Symposium on Fluid Flow Measurement (ISFFM), Querétaro, Mexico, MX, April 2018.

[7] Johnson, A. N., Boyd, J. T., Harman, E., Khalil, M. Ricker, J. R., Crowley, C. J., Wright, J. D., Bryant, R. A., and Shinder, I. I., **Design and Capabilities of NIST's Scale-Model Smokestack Simulator (SMSS),** 9th International Symposium on Fluid Flow Measurement (ISFFM), Arlington, Virginia, April 2015.

[8] Bryant, R. A.; Johnson, A. N.; Wright, J. D.; Wong, T. M.; Whetstone, J. R.; Moldover, M. R.; Shinder, I. I.; Swiggard, S.; Gunning, C.; Elam, D.; Martz, T.; Harman, E.; Nuckols, D.; Zhang, L.; Kang, W.; and Vigil, S.; ***Improving Measurement for Smokestack Emissions - Workshop Summary***, Special Publication (NIST SP) 1228, 9/21/2018.

[9] Johnson, A. N., Shinder, I. I., Moldover, M. R., Boyd, J. T., and Filla, B. J., ***Progress Towards Accurate Monitoring of Flue Gas Emissions*****,** 10th International Symposium on Fluid Flow Measurement (ISFFM), Querétaro, MX, March 2018.

[10] Yeh, T. T., Hall, J. M., *Air Speed Calibration Service*, NIST Special Publication 250-79, National Institute of Standards and Technology, Gaithersburg, Maryland, 2006.

[11] Yeh, T. T., Hall, J. M., ***An Uncertainty Analysis of the NIST Airspeed Standards, ASME Paper FEDSM2007-37560***, ASME/JSME 5th Joint Fluids Engineering Conference, pp. 135-142, San Diego, California, USA, 2007.

[12] Yeh, T. T. and Hall, J. M. ***Uncertainty of NIST Airspeed Calibrations***, *Technical document of Fluid Flow Group*, NIST, Gaithersburg, Maryland, USA, 2008.

[13] Shinder, I. I., Crowley, C. J., Filla, B. J., Moldover, M. R., ***Improvements to NIST's Air Speed Calibration Service***, 16th International Flow Measurement Conference, Flomeko 2013, Paris, France September 24-26, 2013.

[14] Shinder, I. I., Khromchenko, V. B., and Moldover, M. R., ***NIST's New 3D Airspeed Calibration Rig, Addresses Turbulent Flow Measurement Challenges,*** 9th International Symposium on Fluid Flow Measurement (ISFFM), Washington, DC, U. S., April 2015.

[15] Environmental Protection Agency**, *40 CFR Part 60 Application Method 4 Determination of Moisture Content in Stack Gases***, Washington D.C., 1996.

[16] Environmental Protection Agency**, *40 CFR Part 60 Application Method 3A Determination of Oxygen and Carbon Dioxide Concentrations in Emissions From Stationary Sources***, Washington D.C., 1996.